PNAS

Supplementary Information for
Hydration-Mediated G-Protein-Coupled Receptor Activation

Steven D.E. Fried, Kushani S.K. Hewage, Anna R. Eitel, Andrey V. Struts, Nipuna Weerasinghe, Suchithranga M.D.C. Perera, and Michael F. Brown

Michael F. Brown
Email: mfbrown@u.arizona.edu

This PDF file includes:

1. Supplemental Methods

1(a). Purification of rhodopsin in native rod disk membranes (RDM). Retinal disk membranes (RDM) were isolated from bovine retinas under dim red light (Kodak Safelight red filter 1, Eastman Kodak Co.) at 4 °C or on ice, and under a gentle stream of argon gas. Bovine retinas were obtained from a commercial source (W. L. Lawson Co., Omaha, NE, USA) (1). Frozen bovine retinas were thawed and homogenized in a loose-fitting Teflon homogenizer in 30 mL of homogenizing solution (30% w/w sucrose) per 50 retinas. After ten strokes, the resulting homogenate was centrifuged at 2,600 x *g* for 20 min at 4 °C. The pelleted retina fragments were then homogenized in an equal volume of homogenizing solution in a tight-fitting Teflon homogenizer, followed by an additional step of centrifugation at 2,600 x *g* for 20 min at 4 °C. Both supernatants were collected by syringe and combined together with two equal volumes of 10 mM Tris-acetate, pH 7.4, prior to centrifuging at 8,000 x *g* for 50 min at 4 °C. The resulting pellet was resuspended in 1.10 g/mL sucrose density gradient solution, and layered onto discontinuous sucrose step gradients (1.11, 1.13, and 1.15 g/mL with volumes of 10, 10, and 8 mL respectively). Sucrose gradients were centrifuged in polyallomer tubes using a swinging bucket rotor at 113,000 x *g* for 1 h at 4 °C. The band at the interface of the 1.11 g/mL and 1.13 g/mL layers corresponds to the rod disk membranes (RDM), and was collected by syringe. The collected RDM carpets were washed threefold, each time by diluting with two volumes of water double-distilled water, centrifuging at 48,000 x *g* for 30 min at 4 °C, and isolating the pelleted membranes from the aqueous supernatant.

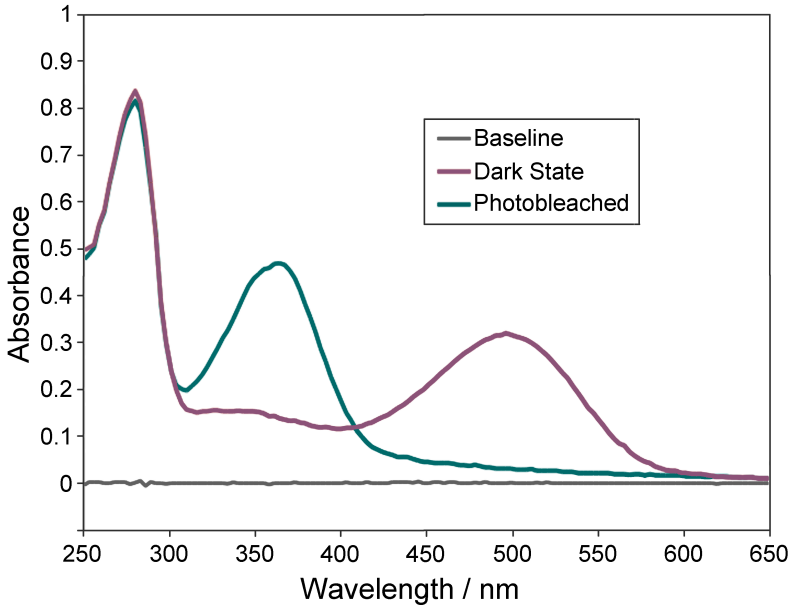

Fig. S1. Purified rhodopsin within its native rod outer segment disk membranes was characterized for purity and concentration using UV-Visible spectroscopy. Samples were dissolved in a 9:1 solution of sodium phosphate buffer / AMMONYX® LO detergent, with 35 mM hydroxylamine hydrochloride. Spectra were recorded of the initial (dark-state) sample as well as the sample after photobleaching with a green LED lamp for 40 s. Dark-state rhodopsin absorbs at 500 nm, while the free retinal from the bleached apoprotein opsin absorbs at 360 nm. The 280 nm absorbance is characteristic of aromatic amino acids including tryptophan and tyrosine. The concentration of rhodopsin is calculated by the A_{500} value, using [Rho] / (mg/mL) = A_{500} (dark) – A_{500} (photobleached). Purity is assessed by the A_{280}/A_{500} ratio, calculated as $[A_{280} - A_{310}]/[A_{500}$ (dark) – A_{500} (photobleached)]. RDM with an A_{280}/A_{500} ratio below 2.7 were routinely used for osmotic stress experiments.

Following the final wash, the membranes were suspended in 67 mM BTP buffer (pH 7.5) containing 130 mM NaCl and 2 mM $MgCl_2$ (rhodopsin concentration ≈ 10 mg/mL) and stored at –80 °C. The purity of rhodopsin was measured by the spectrophotometric A_{280}/ A_{500} ratio which was routinely between 2.4 and 2.7 (Fig. S1). Osmolyte solutions were prepared by weight percent in the same 67 mM BTP, 130 mM NaCl, 2 mM $MgCl_2$ buffer, while the pH was adjusted using 12.1

N HCl or saturated NaOH solution and measured in a 15 °C water bath by a Beckman Φ-340 pH/temp meter equipped with an Accumet pH probe (13-620-299B, Fisher Scientific). For pH titration experiments requiring pH values below 5.8, an acetate buffer was instead used: 67 mM CH_3COONa, 130 mM NaCl, and 2 mM $MgCl_2$. We assumed that osmotic pressure induced by the buffer components was negligible compared to that induced by the addition of osmolytes. Osmolytes included PEG 200, PEG 300, PEG 400, PEG 600, PEG 1000, PEG 1500, PEG 2000, PEG 3000, PEG 4000, PEG 6000, and sucrose (Sigma-Aldrich, St. Louis, MO, USA). To prepare samples, the rhodopsin was removed from –80 °C and was thawed and resuspended in osmolyte solutions to achieve a 10 μM rhodopsin concentration and the correct weight percent (0-60%) of osmolyte. Samples were then sonicated for 90 half-second pulses with a tip sonicator under a continuous stream of argon gas and in an ice bath (Heat Systems Sonicator W-375 Cell Disruptor).

1(b). Data collection and analysis. All spectroscopic measurements were recorded on a Cary 50 UV-Visible spectrophotometer (Varian, Inc., Palo Alto, USA) over the range of 270 nm–610 nm, at a scanning rate of 4800 nm/min. A 1 mm pathlength synthetic quartz cuvette was utilized, with the stage temperature kept constant at 15 °C ± 0.5 °C by a thermostat-regulated water circulator. Samples were incubated five minutes within the cuvette on the sample stage prior to data collection. Twenty spectra of the dark-state rhodopsin sample were recorded prior to bleaching the sample with a green LED lamp (11.6 V array of 40 WEEGN10-CS LEDs with peak wavelength 528 nm, 10000 mcd; Winger, China) for approximately seven seconds. The average dark-state spectrum was subtracted from the average of five photoactivated rhodopsin spectra to generate an experimental difference spectrum reflecting the change in absorbance due to photoactivation. To account for scattering changes after bleaching, the experimental difference spectrum was subjected to an inverse-square wavelength scattering correction using the following equation:

$$\Delta A_{\text{corr}} = \Delta A - a / \lambda^2 + b\,. \tag{1.b.1}$$

Here ΔA_{corr} is the corrected amplitude of the difference spectrum, ΔA is the experimental difference amplitude, a is the fitting constant, λ is the wavelength, and b is an additive constant to correct for baseline shifts. Values of a and b were determined to make the average absorbance change ΔA near 300 nm equal to the average absorbance change near 610 nm. Following the scattering correction, a basis spectral fitting method was utilized to determine the relative fractions of metarhodopsin-I (MI) and metarhodopsin-II (MII). Basis difference spectra were collected by varying pH and temperature conditions to completely favor either the MI or MII state for 10 μM rhodopsin in RDM. MI-favoring conditions were pH 9.2 and 5 °C, while MII-favoring conditions were pH 5.0 and 15 °C. A linear combination of these basis spectra were fit by the method of least squares to the experimental difference spectrum:

$$\Delta A\left(\lambda\right) = c_1 \Delta A_{\text{MI}}\left(\lambda\right) + c_2 \Delta A_{\text{MII}}\left(\lambda\right). \tag{1.b.2}$$

The positive coefficients c_1 and c_2 reflect the relative contributions of either MI or MII to the total photoactivated rhodopsin system. The total normalized MII fraction θ could therefore be calculated as $\theta = c_2/(c_1 + c_2)$, while the equilibrium constant was calculated as $K = c_2/c_1$.

The applicability of the basis spectral fitting analysis was demonstrated by the existence of an isosbestic point within spectral data sets, indicating the presence of two predominant spectral components (main text Fig. 2). To confirm the accuracy of the experimentally collected basis spectra, singular-value decomposition (SVD) was performed on a single matrix constructed from three sets of pH titration spectra (no PEG, 30% PEG 200, and 50% PEG 2000) using Matlab R2018a. Two predominant singular vectors were observed, whose line shapes matched well with the experimentally determined basis spectra.

1(c). Determination of Optimal Sonication Time. Sonication was observed to alter the MII fraction of photoactivated rhodopsin in both PEG-enriched and PEG-free solutions (Fig. S2). In PEG-free environments, these effects are attributed to changes in the lipid membrane properties that govern the metarhodopsin equilibrium. Lower concentrations of small PEGs, such as PEG 200, have a greater likelihood of diffusing across the rod disk membranes and thus prevent

preliminary osmotic pressure effects across the membrane prior to sonication. For large molecular weight PEGs and higher concentrations of PEG 200, however, osmolytes do not achieve a consistent distribution on either side of the membrane and instead produce preliminary osmotic pressure effects across the rod disk membranes prior to sonication. These osmotic effects are expected to induce a membrane deformation and thickening that favor the MII state. Following sonication and redistribution of osmolytes, however, these effects are mitigated and the MII fraction exhibits a net decrease. For four different sets of osmolyte conditions at pH 7.5, sonication effects on the MII fraction exhibit a plateauing effect after 90 half-second pulses, indicating the most complete restructuring of the lipid bilayer and reorganization of the osmolyte distribution is achieved within this time. Therefore, for purposes of this experiment a 90-pulse sonication time was utilized to eliminate transmembrane osmotic pressure effects and isolate the effect of osmotic stress on rhodopsin.

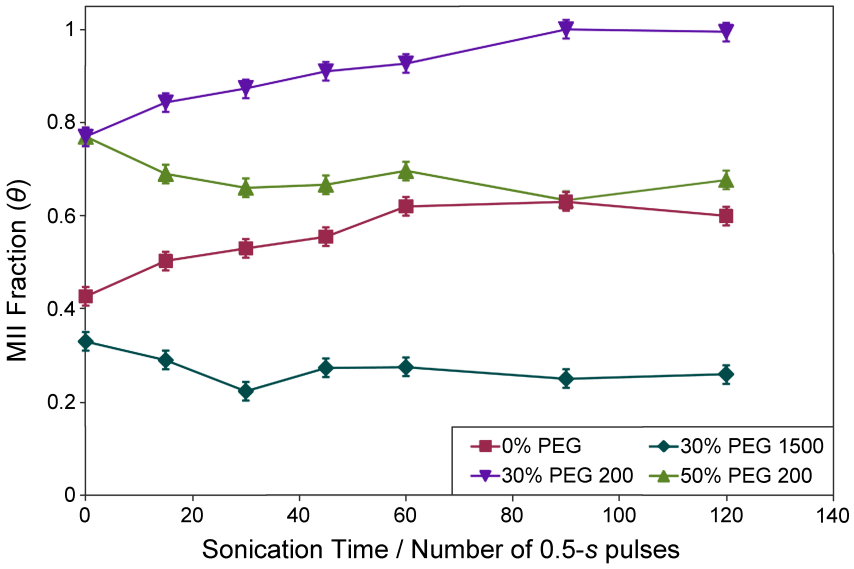

Fig. S2. Effect of sonication time on MII fraction θ for various osmotic conditions. For conditions of no osmolytes or a low concentration of small osmolyte (PEG 200), the MII fraction increases with sonication. For large concentrations of small osmolyte or concentrations of large polymer osmolyte (PEG 1500), the MII fraction decreases with sonication. All sonication effects reach a plateauing effect after 90 pulses, indicating that this was the optimal sonication time to guarantee a homogeneous osmolyte distribution. The deviation in MII fraction between non-equilibrated and fully equilibrated states indicates the possible influence of an additional trans-bilayer osmotic pressure effect in cases where osmolyte is not symmetrically distributed across the membrane.

2. Supplemental Theory

2(a). Dependence of Metarhodopsin Equilibrium on Osmotic Stress. The metarhodopsin equilibrium is governed by the Gibbs free energy of the hydrated protein system, and thus may be perturbed by the natural variables temperature and pressure according to the thermodynamic relation $dG = VdP - SdT$. Under isothermal conditions such as those encountered here, we may consider the relation $(\partial G/\partial P)_T = V$ to understand how the Gibbs free energy may be perturbed by either hydrostatic pressure P, or, by analogy, the osmotic pressure Π. This requires us to first understand the relationship between volume and pressure (or osmotic pressure). We shall pursue this in two ways, first through a more general formulation involving a virial expansion, and later by a more specific case involving compressibility of a fluid.

Consider first a canonical virial expansion of the thermodynamic compressibility factor Z:

$$Z = \frac{P\bar{V}}{RT}\left(1 + \frac{B'}{\bar{V}} + \frac{C'}{\bar{V}^2} + ...\right). \tag{2.a.1}$$

We can express molar volume as a virial expansion in terms of pressure via algebraic rearrangement:

$$\bar{V} = \frac{RT}{P}(1 + BP + CP^2 + ...). \tag{2.a.2}$$

Here, $B = B'/RT$ and $C = (C' - B'^2)/(RT)^2$, etc., meaning the coefficients of both expressions may be expressed in terms of one another. This expression can denote the molar volume for a particular protein state at constant hydrostatic and osmotic pressures. Note then, that for a difference in volume to occur between the MI and MII states, there must be an associated change in the virial coefficients, of which B is the most important. These virial coefficients therefore contain all necessary information describing the deviation of either hydrated protein state from the ideal gas case. Therefore at the most general level, volume changes, compressibility changes, as well as changes in attractive and repulsive forces will all be linked in some manner to the deviations in virial coefficients between the two protein states.

To calculate the influence of osmotic pressure on the molar Gibbs free energy, we use the aforementioned relation for the partial molar case $(\partial\bar{G}/\partial P)_T = \bar{V}$ and integrate the volume expression with respect to pressure P over the perturbation in osmotic pressure Π from a reference state Π_0.

$$\int_{\Pi_0}^{\Pi} d\bar{G} = \int_{\Pi_0}^{\Pi} \bar{V}dP = \int_{\Pi_0}^{\Pi} (RT/P + BRT + CRTP + ...)dP. \tag{2.a.3}$$

Hence the new Gibbs free energy of a single, hydrated protein state after applying osmotic pressure is as follows:

$$\bar{G}(\Pi) = \bar{G}(\Pi_0) + RT\ln\left(\Pi/\Pi_0\right) + BRT\left(\Pi - \Pi_0\right) + \tfrac{1}{2}CRT\left(\Pi^2 - \Pi_0^2\right) + ... \tag{2.a.4}$$

Momentarily recall that the unperturbed volume expressed in terms of the reference osmotic pressure is the following:

$$\bar{V}_0 = \frac{RT}{\Pi_0} + BRT + CRT\Pi_0 + ... \tag{2.a.5}$$

Such an expression can apply to either the MI or MII states, where B is the most important coefficient toward expressing a linear, volume-dependent osmotic stress effect on the free energy. Higher-order terms remain to account for the fact that not all virial coefficients may change synchronously with volume (for instance, in the case of a change in isothermal compressibility $\Delta\kappa$ as we shall see shortly). To second order, we need only consider the virial coefficient C in addition to the volume changes. In light of this observation, we substitute equation 2.a.5 describing the reference state, plus a similar one for the final (perturbed) state $(\Pi, \bar{V})$, back into equation 2.a.4:

$$\bar{G}(\Pi) = \bar{G}(\Pi_0) + RT\ln\left(\Pi/\Pi_0\right) + \left(\Pi\bar{V} - \Pi_0\bar{V}_0\right) - \tfrac{1}{2}CRT\left(\Pi^2 - \Pi_0^2\right) + ... \tag{2.a.6}$$

Now we may consider the two-state transition of rhodopsin, an equilibrium between the MI and MII states. The standard *change* in molar free energy $\Delta G°$ of this process under applied osmotic stress may therefore be expressed as a change in each of the constituent terms of $\bar{G}(\Pi)$ resulting from the MI to MII transition:

$$\Delta G^{o}(\Pi) = \Delta G^{o}(\Pi_0) + \Delta\left[RT\ln\left(\Pi/\Pi_0\right)\right] + \Delta\left[\left(\Pi\bar{V} - \Pi_0\bar{V}_0\right)\right] - \Delta\left[\tfrac{1}{2}CRT\left(\Pi^2 - \Pi_0^2\right)\right] + ... \tag{2.a.7}$$

The term $RT\ln(\Pi/\Pi_0)$ does not change between the MI and MII states, and so vanishes. For the other terms, we can take the osmotic pressure change with reference to zero osmotic pressure ($\Pi_0 = 0$):

$$\Delta G^{o}(\Pi) = \Delta G^{o} + \Delta\left(\Pi\bar{V}\right) - \Delta\left(\tfrac{1}{2}CRT\Pi^{2}\right) + \ldots \quad (2.a.8)$$

We can assume that in the first-order term, the deviation between $\bar{V}_0$ and $\bar{V}$ is small (low compressibility of the protein hydration volume) in comparison to the change in volume ΔV^{o} between the MI and MII states under standard state (zero osmotic pressure) conditions. Then perturbations to the relative molar Gibbs free energy difference between MI and MII can be expressed in terms of ΔV^{o} and ΔC to second order:

$$\Delta G^{o}(\Pi) = \Delta G^{o} + \Pi\Delta V^{o} - \tfrac{1}{2}RT\Pi^{2}\Delta C\,. \quad (2.a.9)$$

Finally, the change in molar free energy is related to the equilibrium constant under standard (zero osmotic pressure) and perturbed conditions via $\Delta G^{o} = -RT\ln K$. Employing this substitution, then the final function to which we fit our observed metarhodopsin equilibria under varied osmotic pressure is the following:

$$\ln K = \ln K^{o} - (\Delta V^{o}/RT)\Pi + (\tfrac{1}{2}\Delta C)\Pi^{2} \quad (2.a.10)$$

where K is the equilibrium constant perturbed by osmotic pressure Π and K^{o} is the unperturbed constant under zero osmotic pressure.

Note that the linear term of this function is proportional to the hydrated volume change of rhodopsin under standard conditions, from which the apparent number of bulk water molecules entering the protein environ (presumably the transducin binding cleft) during the MI-MII transition may be calculated. The second-order term, governing the curvature of the behavior, is proportional to the apparent change in the virial coefficient C. It is important to note that this virial coefficient describes the non-ideality of the collective, hydrated protein *system*, and is the most general mathematical treatment of the deviation from linearity observed for osmotic stress perturbation of the rhodopsin conformational equilibrium.

In a slightly alternate approach, and more specific to the phenomenon of compressibility change, an applied osmotic pressure can generate two major effects within a system. These consist of a shift in chemical equilibrium to favor species of lower free energy under higher pressure, and a physical change in volume proportional to the compressibility of those species. The latter of these is dictated by an osmotic compressibility constant κ_Π for the water associated with the protein, defined as $\kappa_\Pi \equiv -(\partial\ln V/\partial\Pi)_T$ (2). Separating the variables and integrating with respect to osmotic pressure, we derive an expression for volume of the macromolecule hydration as a function of osmotic pressure:

$$V = V_0 e^{-\kappa_\Pi(\Pi-\Pi_0)}. \quad (2.a.11)$$

This function may then be substituted into a differential expression for the Gibbs free energy at constant temperature T, and integrated with respect to pressure in direct analogy to 2.a.3:

$$\int_{\Pi_0}^{\Pi} d\bar{G} = \int_{\Pi_0}^{\Pi} \bar{V}d\Pi' = \int_{\Pi_0}^{\Pi} \bar{V}_0 e^{-\kappa_\Pi(\Pi'-\Pi_0)}d\Pi'. \quad (2.a.12)$$

Hence the partial free energy per mole of the hydrated protein state perturbed by osmotic pressure is as follows:

$$\bar{G}\left(\Pi\right) = \bar{G}\left(\Pi_0\right) - \left(\bar{V}_0/\kappa_\Pi\right)\left(e^{-\kappa_\Pi(\Pi-\Pi_0)} - 1\right) \quad (2.a.13)$$

Note that the resulting function may be expanded as a Taylor series about the reference osmotic pressure Π_0:

$$\bar{G}(\Pi) = \bar{G}(\Pi_0) + \bar{V}_0(\Pi - \Pi_0) - \tfrac{1}{2}\bar{V}_0\kappa_\Pi(\Pi - \Pi_0)^2 + \ldots \quad (2.a.14)$$

We may set the reference osmotic pressure of the system Π_0 to zero as before. Next, we may consider the two-state transition of rhodopsin, a chemical equilibrium between the MI and MII states. The change in free energy $\Delta G°$ of this process under applied osmotic stress may therefore be expressed:

$$\Delta G^\circ(\Pi) = \Delta G^\circ + \Delta V^\circ \Pi - \tfrac{1}{2}\Delta(\bar{V}_0\kappa_\Pi)\Pi^2 + \ldots \quad (2.a.15)$$

In view of the substantial variability in κ_Π for closely related biopolymers in various hydration states (2), we may assume that the *relative* change in rhodopsin hydration volume upon MII formation is negligible compared to the relative osmotic compressibility change from a dehydrated to hydrated state. Thus, we ignore the $\kappa_\Pi\Delta\bar{V}_0$ term and leave the $\bar{V}_0\Delta\kappa_\Pi$ term, because the apparent change in compressibility of the water volume around the protein may be suitably large in the event of the MI to MII transition. We likewise make a second-order approximation, disregarding the subsequent terms:

$$\Delta G^\circ(\Pi) = \Delta G^\circ + \Delta V^\circ \Pi - \tfrac{1}{2}(\bar{V}_0\Delta\kappa_\Pi)\Pi^2 . \quad (2.a.16)$$

Finally, the change in free energy is related to the equilibrium under osmotic stress as before, giving an analogue equation to 2.a.10:

$$\ln K = \ln K^\circ - \left(\Delta V^\circ / RT\right)\Pi + \tfrac{1}{2}\left(\bar{V}_0\Delta\kappa_\Pi / RT\right)\Pi^2 . \quad (2.a.17)$$

Note that the linear term of this function is again proportional to the hydrated volume change of rhodopsin under standard conditions, while now the second-order term is more specifically proportional to the apparent change in compressibility of the water volume around the protein during the activation process.

As a final note showing the robustness of these equations with respect to the activation mechanism used, we consider than in the rhodopsin system, the equilibrium is defined between MI, with protonated retinylidene Schiff base, and MII, with a deprotonated Schiff base. Yet the MII state exists in multiple forms according to the protonation state of Glu[134], as rhodopsin activation is currently understood to follow the mechanism Rh + *hν* → MI⇌ MII_a ⇌ MII_b + H_3O^+ ⇌ MII_bH^+ (3). Since all substates of MII are indistinguishable to UV-Visible spectroscopy, we can simplify the problem by considering two equilibria, the first between MI and either MII_a or MII_b (identical for the purposes of UV-Visible quantification), and the second between MI and the protonated MII_bH^+. For the first possible equilibrium, we have $K_{12} = [\mathrm{MII_{a/b}}]/[\mathrm{MI}]$. Since this equilibrium is unimolecular (only involving a conformational change in rhodopsin), then this equilibrium is pH-independent and we can insert it into equation 2.a.18 with an isomorphic result:

$$\ln K_{12} = \ln K_{12}^\circ - \left(\Delta V^\circ / RT\right)\Pi + \tfrac{1}{2}\left(\bar{V}_0\Delta\kappa_\Pi / RT\right)\Pi^2 . \quad (2.a.18)$$

Consider, however, a subsequent equilibrium that is pH-dependent, defined by $K_3 = [\mathrm{MII_b \cdot H^+}]/([\mathrm{MI}][\mathrm{H^+}])$. We can relate this formal equilibrium constant to an observed constant $K_3' = [\mathrm{MII_b \cdot H^+}]/[\mathrm{MI}]$, where the identity $\ln K_3' = \ln K_3 + 2.303\mathrm{pH}$ must hold. Now substituting into equation 2.a.18, we obtain the following:

$$\ln K_3' = \ln K_3^\circ + 2.303\mathrm{pH} - \left(\Delta V^\circ / RT\right)\Pi + \tfrac{1}{2}\left(\bar{V}_0\Delta\kappa_\Pi / RT\right)\Pi^2 . \quad (2.a.19)$$

In this case, the pH factor is absorbed into the scalar term of the quadratic expression without impacting the linear or quadratic terms. Thus in either case, fitting a quadratic function to the dependency of the spectroscopically measured equilibrium [MII]/[MI] will yield first and second-order terms from which the relevant thermodynamic data may be calculated, showing the model-independence of the osmotic stress approach.

2(b). Osmotic Pressure Calculation and Error Propagation for $\ln K$ and θ. For a particular osmotic environment, spectroscopic measurements of the MII fraction θ were recorded in triplicate using three different samples of rod outer segment suspension. For the osmotic pressure response curves, the error in $\ln K$ was propagated from two primary sources: the error in the spectroscopic measurement of θ (taken to be $\varepsilon_{\theta,\exp}$ = 0.02, the standard deviation of θ in the absence of osmolyte at pH 7.5 for all experimental trials), and the error in calculated osmotic pressure. PEG-induced osmotic pressures were calculated by a universal fitting equation derived from experimentally observed osmotic pressures (4).

$$\Pi = \frac{\alpha^{4/5} RT}{N^{9/5} M_{\mathrm{m}} \bar{V}} \left(\frac{\gamma}{\gamma^{\#}} + \left(\frac{\gamma}{\gamma^{\#}} \right)^{9/5} \right). \tag{2.b.1}$$

Here, α is an experimentally determined numerical prefactor, M_{m} is the molecular weight of the PEG monomer, N is the number of monomers in a polymer chain, $\bar{V}$ is the partial molar volume of PEG, γ is the polymer mass concentration, and $\gamma^{\#}$ is the crossover concentration between ideal and non-ideal behavior calculated as

$$\gamma^{\#} = \left(\alpha^{-4/5} N^{-4/5} \right) / \bar{V} \,. \tag{2.b.2}$$

Hence, the accuracy of the model in fitting the osmotic pressure of any sized PEG hinges upon a single experimentally determined parameter α, where for a PEG/water system, α = 0.49 ± 0.01. Therefore, the error of $\ln K$ due to error in calculated osmotic pressure has its source in the error ε_α = 0.01, meaning the net error in $\ln K$, denoted $\varepsilon_{\ln K}$, may be calculated as follows:

$$\varepsilon_{\ln K}^2 = \left(\varepsilon_{\theta,\,\exp} \frac{\partial \ln K}{\partial \theta_{\mathrm{meas}}} \right)^2 + \left(\varepsilon_\alpha \frac{\partial \ln K}{\partial \Pi} \frac{\partial \Pi}{\partial \alpha} \right)^2 . \tag{2.b.3}$$

Partial derivatives have been approximated numerically to derive the error bars shown in Figures 2 and 3 of the main text. To aid visualization by considering error along only one axis at a time, the error in osmotic pressure was propagated to an error in $\ln K$ by partial derivatives. As an approximation for the true behavior, the piecewise modeled dependence of $\ln K$ on osmotic pressure for each osmolyte was used in error propagation—quadratic regression equations for large osmolytes and for small osmolytes above the saturation point, and a linear regression for small osmolytes prior to the saturation point.

Titration curve errors in θ are assumed to depend on two types of error: that of the pH and that of the measurement in θ. The intrinsic error in the measurement in theta is again assumed to be 0.02. The pH error is taken to be 0.1 pH unit, while the derivative of θ with respect to pH is given by the double pK_A and alkaline endpoint Henderson-Hasselbalch titration curve (see section 2d)

$$\theta(\mathrm{pH}) = \frac{1 + K_3[\mathrm{H}^+]}{\theta_{\mathrm{alk}}^{-1} + K_3[\mathrm{H}^+] + K_4[\mathrm{H}^+] + K_3 K_4 [\mathrm{H}^+]^2} \,. \tag{2.b.4}$$

Therefore, the net error in θ for a point on a pH titration curve is given as the following:

$$\varepsilon_\theta^2 = \varepsilon_{\theta,\mathrm{meas}}^2 + \left(\varepsilon_{\mathrm{pH}} \frac{\partial \theta}{\partial \mathrm{pH}} \right)^2 . \tag{2.b.5}$$

These error values have been plotted as error bars on Figure 4 of the main text.

2(c). Calculating Number of Waters and ΔC. A second-degree polynomial was fit to the osmotic-pressure dependent data for each sized PEG (Tables S1–S4). For large molecular weight PEGs, individual data sets were used for curve fitting in their entireties, while for small molecular weight PEGs, only those data illustrating a quadratic trend following the $\ln K$ maximum (saturation

point) were used for curve fitting. Nonlinear regression was performed in Matlab R2018a using a nonlinear least squares algorithm. A standard-state volume change ΔV^{o} for the MI-MII transition was calculated (eq. 2.a.10) by multiplying the linear term coefficient by the gas constant R and temperature T. Using the partial molar volume of water $\bar{V}_W$, the number of water molecules N_W penetrating into rhodopsin under standard state conditions for a particular molecular weight PEG is calculated by $N_W = \Delta V^{o}$. The regression-calculated standard errors were similarly scaled to reflect the error in calculated water influx. Similarly, a standard change in virial coefficient ΔC for the MI-MII transition for each molecular weight PEG was calculated from the best-fit quadratic term coefficients (eq. 2.a.10), which can likewise be converted to an estimated compressibility change (eq. 2.a.18). For the initial protein hydration volume $\bar{V}_0$, an estimated value of 34.4 L/mol was used based on the crystal structure of dark-state rhodopsin (5, 6). Standard errors in the second-degree fitted term were similarly scaled to reflect changes in compressibility for each size of polymer. Results for the number of water molecules and change in compressibility are reported in Table S5 and plotted in Figure 1 of the main text.

2(d). Reproducibility of Osmotic Stress Effects. Similar osmotic pressure dependencies have been noted at different pH values for PEG 200 and for PEG 1500 (Fig. S3). For varying osmotic pressures at pH 7.5 and at pH 8.5, PEG 200 induces a similar trend of a linearly increasing MII fraction until 30–35% (w/w) PEG 200, after which $\ln K$ decreases quadratically with osmotic pressure similarly to what was seen for large molecular weight PEGs. The PEG 1500, on the other hand, produces a purely quadratic trend in $\ln K$ as a function of applied osmotic pressure for both pH 7.5 and pH 6.5. In both situations, the difference in pH causes predominantly only a vertical shift towards higher MII fraction with lower pH.

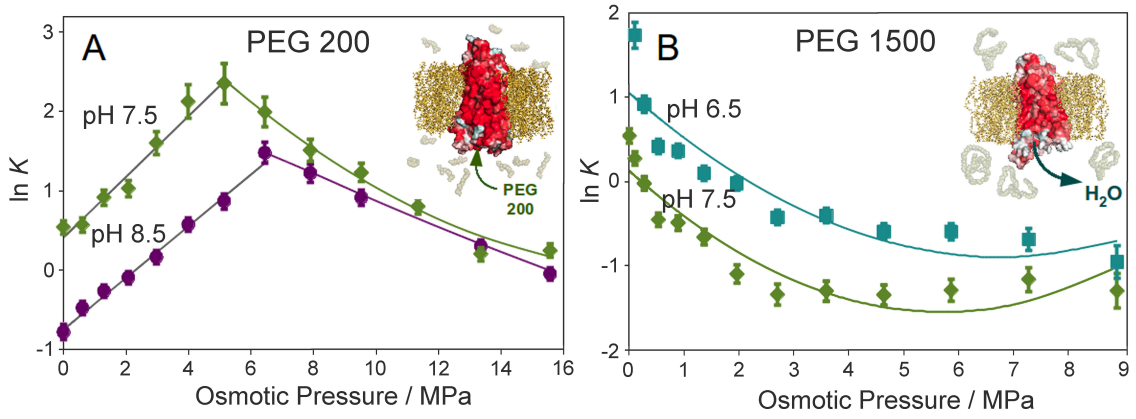

Fig. S3. Osmotic pressure effects on rhodopsin were reproducible at varying pH conditions. (A) At two different pH values, the response of ln *K* to osmotic stress induced by PEG 200 is initially linear towards increasing MII before a saturation point, after which an osmotic behavior occurs, tending toward MI as a quadratic function of osmotic pressure. The higher pH vertically shifts the curve to lower ln *K*. **(B)** The response of ln *K* to osmotic pressure induced by PEG 1500 is quadratic at two different pHs, where the lower pH vertically shifts the curve to higher ln *K*.

Moreover, the PEG 200 results were found to be reproducible at different temperatures (15 °C and 8 °C) as well as different concentrations of rhodopsin in RDM (5, 10, and 15 μM) (Fig. S4). In each case, a sudden reversal in the response of rhodopsin to increasing concentrations of small osmolyte was observed: the initial linear shift to MII reversed after a saturation point, shifting back to MI with an approximate quadratic dependence of $\ln K$ on osmotic pressure. The lower temperature results were particularly useful in confirming this phenomenon, as lower temperatures led to significantly smaller errors inherent to the resulting measurements. Of some ambiguity yet is the significance of the robustness of the PEG 200 results with respect to the rhodopsin

concentration. In the case of a specific interaction between PEG and rhodopsin, it would be expected that the saturating concentration of PEG 200, at which point the trend reversal occurs, would vary proportionally to the rhodopsin concentration. However, this effect is clearly not observed. The most plausible explanation is that at such high concentrations of PEG 200 as those used here, the solution thermodynamics transition into a realm of non-ideality at which point minor perturbations in the rhodopsin concentration have little effect on the macro-scale interactions between receptor and polymer in the bulk solution.

An additional osmolyte, sucrose, was tested as a comparison to the findings of Mitchell et al. (7, 8). Measuring the effects of the osmolyte on the metarhodopsin equilibrium using calculated osmotic pressures (9), we observed that the logarithm of the equilibrium constant shifted approximately linearly to higher MII fractions with increasing osmotic pressures, and that no saturation point was achieved (Fig. S5). We interpret these results in light of the fact that sucrose has lower conformational entropy compared to polymer osmolytes such as small polyethylene glycols. As a result, the saturating limit of sucrose penetrating into rhodopsin is not achieved below 60% (w/w) sucrose.

Our findings are further substantiated by testing the effects of intermediate polymer sizes on the pH dependence of rhodopsin activation (Fig. S6). These intermediate polymer sizes (30% PEG 300 and 50% PEG 600) induce shifts in the rhodopsin titration curve in between those observed for the largest osmolytes (50% PEG 1000, 2000, and 40000) and the smallest osmolyte (30% PEG 200). For these intermediate-sized osmolytes, there is some deviation between the experimental values and the best fit to the theoretical curve, which typically demonstrate a lower metarhodopsin-II fraction at lower pHs than the expected values. The reason for this trend is not yet well-understood but may be in part explained by the presence of other substates in the energy landscape equilibrium possessing a protonated Schiff base that decrease the apparent MII fraction at these pHs.

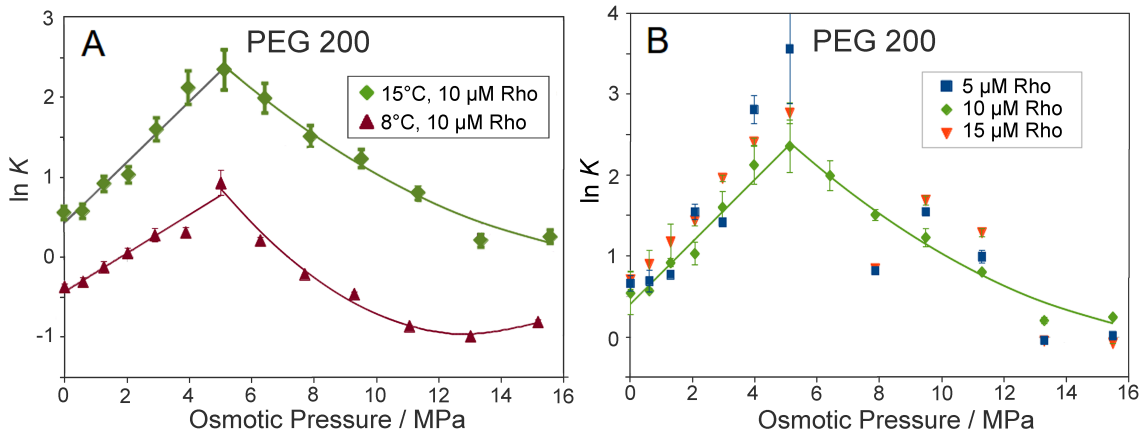

Fig. S4. PEG 200 results exhibited reproducibility at different (A) temperatures (15 °C vs 8 °C) and (B) ratios of rhodopsin to osmolyte. In all cases, a sudden reversal in the response of rhodopsin to increasing concentrations of small osmolyte was observed: the initial linear shift to MII gave way after a saturation point to an osmotic back shift characterized by a quadratic dependence of ln *K* on osmotic pressure.

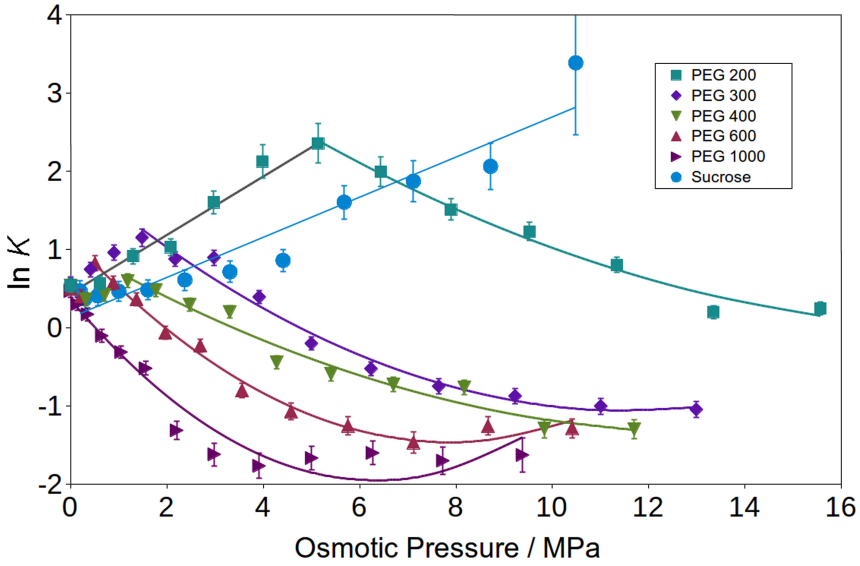

Fig. S5. The response of ln *K* to small PEG osmolytes, as well as the osmolyte sucrose. Sucrose additionally caused a forward shift in the metarhodopsin equilibrium to MII. However, this observed trend was monotonic, unlike for the PEG osmolytes. We interpret these results in light of the lower conformational entropy of sucrose compared to the polymer osmolytes, which allow higher concentrations of sucrose to fit inside of rhodopsin before a saturation point is achieved. The difference in slope for the initial trend of ln *K* versus osmotic pressure is due to differences in affinities between the PEG and sucrose osmolytes for rhodopsin.

2(e). Derivation of pH-dependent Rhodopsin Equilibrium Model. To derive a model of the pH-dependent rhodopsin activation as monitored by UV-Visible spectroscopy, we initially consider the following reaction scheme as reflective of Mahalingam et al. (10):

$$MI_{PSB} \overset{K_1}{\rightleftharpoons} MII_{a\ SB} \overset{K_2}{\rightleftharpoons} MII_{b\ SB} \overset{H^+,\ K_3}{\rightleftharpoons} MII^{+}_{SB}$$

Here, the equilibrium constants are defined as $K_1 = [\mathrm{MII_{a\ SB}}]/[\mathrm{MI_{PSB}}]$, $K_2 = [\mathrm{MII_{b\ SB}}]/[\mathrm{MII_{a\ SB}}]$, and $K_3 = [\mathrm{MII^{+}_{SB}}]/[\mathrm{MII_{b\ SB}}][\mathrm{H^+}]$. Hence, K_1 designates the breaking of the first ionic lock between the retinal Schiff base and Glu^{113}, K_2 represents the equilibrium of the transmembrane helix 6 movement, and K_3 represents the protonation of Glu^{134} and breaking of the second ionic lock to stabilize the activated MII state. Since the substates $MII_{a\ SB}$ and $MII_{b\ SB}$ are both characterized by a deprotonated retinal Schiff base, they are indistinguishable by UV-Visible spectroscopy. We may therefore simplify the reaction scheme by combining the first two equilibria as $K_{12} = [\mathrm{MII_{b\ SB}}]/[\mathrm{MI_{PSB}}]$ and ignoring the $MII_{a\ SB}$ substate. The reaction mechanism is complicated by the fact that the retinal Schiff base also undergoes pH-dependent protonation or deprotonation, which impacts the apparent fraction of active MII rhodopsin measured by UV-Visible spectroscopy. We assume that this reaction occurs independently from the protonation of Glu^{134} and is described by the equilibrium constant K_4 for the forwards (protonation) reaction. The deprotonation of the MI Schiff base is assumed to be negligible over the pH range utilized. We therefore have the following reaction scheme, governed by three independent equilibrium constants:

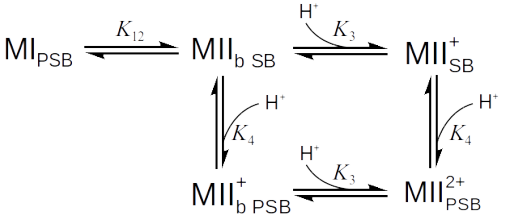

We consider the normalized concentrations of all possible metarhodopsin substates:

$$[\mathrm{MI_{PSB}}]+[\mathrm{MII_{b\,SB}}]+[\mathrm{MII^{+}_{SB}}]+[\mathrm{MII^{+}_{b\,PSB}}]+[\mathrm{MII^{2+}_{PSB}}]=1 \quad (2.e.1)$$

The normalized concentrations of each substate may therefore be expressed as $[\mathrm{MI_{PSB}}] = 1/Z$, $[\mathrm{MII_{b\,SB}}] = K_{12}/Z$, $[\mathrm{MII^{+}_{SB}}] = K_{12}K_3[\mathrm{H^+}]/Z$, $[\mathrm{MII^{+}_{b\,PSB}}] = K_{12}K_4[\mathrm{H^+}]/Z$, and $[\mathrm{MII^{2+}_{b\,PSB}}] = K_{12}K_3K_4[\mathrm{H^+}]^2/Z$, where $Z = 1 + K_{12} + K_{12}K_3[\mathrm{H^+}] + K_{12}K_4[\mathrm{H^+}] + K_{12}K_3K_4[\mathrm{H^+}]^2$.

Using UV-Visible spectroscopy, the fraction of metarhodopsin with deprotonated Schiff base is calculated:

$$\theta([\mathrm{H^+}]) = [\mathrm{MII_{b\,SB}}]+[\mathrm{MII^{+}_{SB}}] = \frac{K_{12}+K_{12}K_3[\mathrm{H^+}]}{1+K_{12}+K_{12}K_3[\mathrm{H^+}]+K_{12}K_4[\mathrm{H^+}]+K_{12}K_3K_4[\mathrm{H^+}]^2}. \quad (2.e.2)$$

Under highly basic conditions, the concentration of hydronium ions approaches zero to give an alkaline endpoint, $\theta_{\mathrm{alk}} = K_{12}/(1+K_{12})$. Substituting this expression into eq. 2.e.2, and subsequent cancellations results in the following:

$$\theta([\mathrm{H^+}]) = \frac{1+K_3[\mathrm{H^+}]}{\theta_{\mathrm{alk}}^{-1}+K_3[\mathrm{H^+}]+K_4[\mathrm{H^+}]+K_3K_4[\mathrm{H^+}]^2}. \quad (2.e.3)$$

Next, the equation is expressed in terms of the pH and the model pK_A values for reactions K_3 and K_4 involving Glu[134] and the retinal Schiff base, where $\mathrm{p}K_{\mathrm{A3}} = -\log(1/K_3) = \log(K_3)$ and $\mathrm{p}K_{\mathrm{A4}} = -\log(1/K_4) = \log(K_4)$. The UV-Visible apparent active metarhodopsin fraction θ is therefore expressed as a function of pH:

$$\theta(\mathrm{pH}) = \frac{1+10^{\mathrm{p}K_{\mathrm{A3}}-\mathrm{pH}}}{\theta_{\mathrm{alk}}^{-1}+10^{\mathrm{p}K_{\mathrm{A3}}-\mathrm{pH}}+10^{\mathrm{p}K_{\mathrm{A4}}-\mathrm{pH}}+10^{\mathrm{p}K_{\mathrm{A3}}+\mathrm{p}K_{\mathrm{A4}}-2\mathrm{pH}}}. \quad (2.e.4)$$

This equation gives the pH-dependence in terms of the model pK_A values as defined with respect to the original reaction scheme equilibrium constants. However, due to the phenomenological presence of the alkaline endpoint, it makes sense to define an *apparent* pK_A value for Glu[134], which will better reflect the pH values demarcating conditions where one rhodopsin species is more abundant versus another. We define the apparent pK_A value of Glu[134] as $\mathrm{p}K_{\mathrm{A,Glu}} = \log(\theta_{\mathrm{alk}}) + \mathrm{p}K_{\mathrm{A3}}$, while the apparent p$K_A$ value of the retinal Schiff base is not affected by the alkaline endpoint value, and thus may be related back to the original reaction mechanism by $\mathrm{p}K_{\mathrm{A,SB}} = \mathrm{p}K_{\mathrm{A4}}$. Substituting these constants into eq. 2.e.4 gives the following:

$$\theta(\mathrm{pH}) = \frac{\theta_{\mathrm{alk}}+10^{\mathrm{p}K_{\mathrm{A,Glu}}-\mathrm{pH}}}{1+\left(1+10^{\mathrm{p}K_{\mathrm{A,SB}}-\mathrm{pH}}\right)10^{\mathrm{p}K_{\mathrm{A,Glu}}-\mathrm{pH}}+\theta_{\mathrm{alk}}10^{\mathrm{p}K_{\mathrm{A,SB}}-\mathrm{pH}}}. \quad (2.e.5)$$

Note that the final term in the denominator $\theta_{\mathrm{alk}}10^{\mathrm{p}K_{\mathrm{A,SB}}-\mathrm{pH}}$ is negligible compared to the other terms at all pH levels and may be typically omitted. Hence, we may write the following:

$$\theta(\mathrm{pH}) = \frac{\theta_{\mathrm{alk}}+10^{\mathrm{p}K_{\mathrm{A,Glu}}-\mathrm{pH}}}{1+\left(1+10^{\mathrm{p}K_{\mathrm{A,SB}}-\mathrm{pH}}\right)10^{\mathrm{p}K_{\mathrm{A,Glu}}-\mathrm{pH}}}. \quad (2.e.6)$$

This three-parameter model follows naturally as an extension of that reported in Mahalingam et al. (10), and was used to fit the pH-dependent UV-Visible data (Fig. S6, Tables S6 and S7).

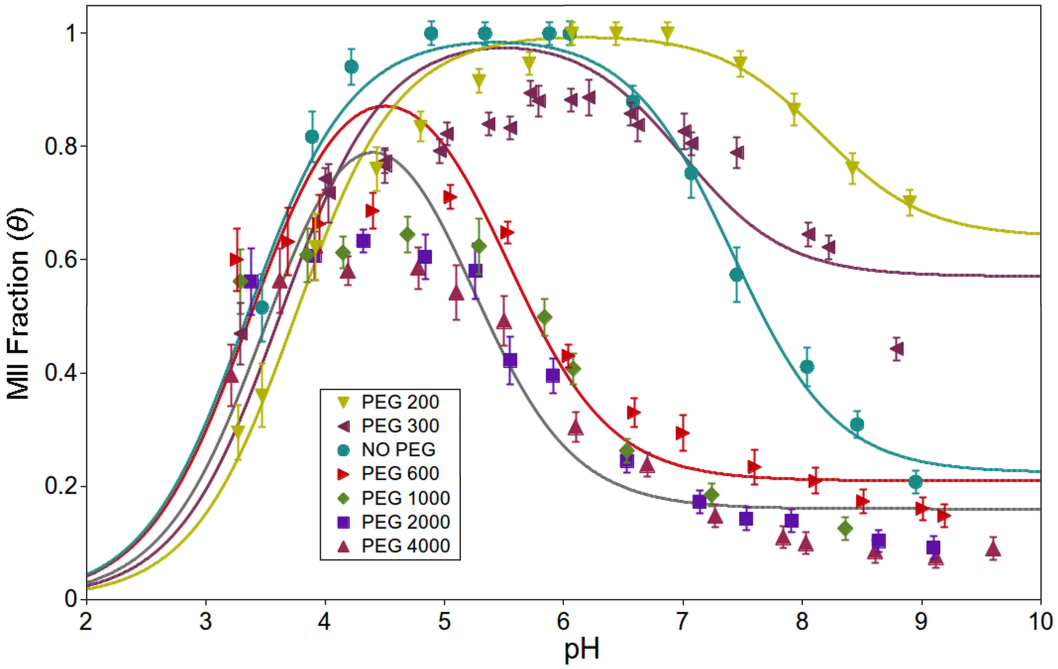

Fig. S6. Additional pH titration curves are shown for the osmolytes 30% PEG 300 and 50% PEG 600, in comparison to the universal 50% large PEG (1000, 2000, 4000) and 30% PEG 200 titration curves given in Figure 6 of the main text. Intermediate osmolyte sizes shift the titration curve partially between the PEG 200 and large 50% PEG curves.

3. Supplemental Data Tables

Table S1. Small Osmolyte Effects on ln *K* by Concentration

PEG 200				PEG 300		
Wt%	Calc. Π / MPa *	pH 7.5 ln *K* †	pH 8.5 ln *K* †	Wt%	Calc. Π / MPa *	ln *K* †
0.00	0.00	0.54 ± 0.09	−0.79 ± 0.09	0.00	0.00	0.56 ± 0.09
4.83	0.61	0.57 ± 0.09	−0.48 ± 0.08	4.83	0.41	0.74 ± 0.09
9.67	1.30	0.91 ± 0.10	−0.27 ± 0.08	9.67	0.90	0.96 ± 0.10
14.50	2.08	1.03 ± 0.10	−0.10 ± 0.08	14.50	1.48	1.15 ± 0.11
19.33	2.97	1.60 ± 0.14	0.16 ± 0.08	19.33	2.17	0.88 ± 0.10
24.17	3.99	2.12 ± 0.21	0.57 ± 0.09	24.17	2.98	0.89 ± 0.10
29.00	5.14	2.35 ± 0.26	0.87 ± 0.10	29.00	3.91	0.39 ± 0.08
33.83	6.44	1.99 ± 0.19	1.48 ± 0.13	33.83	5.00	−0.20 ± 0.08
38.67	7.90	1.51 ± 0.14	1.22 ± 0.11	38.67	6.24	−0.53 ± 0.09
43.50	9.53	1.23 ± 0.12	0.91 ± 0.10	43.50	7.64	−0.75 ± 0.09
48.33	11.34	0.80 ± 0.10		48.33	9.23	−0.88 ± 0.10
53.17	13.35	0.20 ± 0.08	0.30 ± 0.08	53.17	11.01	−1.00 ± 0.10
58.00	15.57	0.24 ± 0.08	−0.05 ± 0.08	58.00	12.99	−1.05 ± 0.10

* Osmotic pressure calculated using equations 2.b.1 and 2.b.2

† ln *K* value determined using the methods described in section 1(b), with errors propagated from equation 2.b.3.

Table S2. Additional Small Osmolyte Effects on ln *K* by Concentration								
PEG 400			**PEG 600**			**Sucrose**		
Wt%	Calc. Π / MPa *	ln *K* †	Wt%	Calc. Π / MPa *	ln *K* †	Wt%	Calc. Π / MPa *	ln *K* †
0.00	0.00	0.54 ± 0.09	0.00	0.00	0.50 ± 0.09	0.00	0.19	0.47 ± 0.13
4.83	0.32	0.36 ± 0.08	4.83	0.22	0.40 ± 0.08	4.83	0.30	0.37 ± 0.12
9.67	0.70	0.42 ± 0.08	9.67	0.51	0.82 ± 0.09	9.67	0.56	0.41 ± 0.12
14.50	1.18	0.60 ± 0.09	14.50	0.89	0.57 ± 0.09	14.50	1.00	0.46 ± 0.13
19.33	1.77	0.48 ± 0.08	19.33	1.37	0.36 ± 0.08	19.33	1.60	0.48 ± 0.13
24.17	2.47	0.29 ± 0.08	24.17	1.97	−0.07 ± 0.08	24.17	2.37	0.61 ± 0.13
29.00	3.30	0.20 ± 0.08	29.00	2.69	−0.23 ± 0.08	29.00	3.31	0.71 ± 0.14
33.83	4.28	−0.44 ± 0.08	33.83	3.56	−0.80 ± 0.09	33.83	4.41	0.86 ± 0.14
38.67	5.41	−0.59 ± 0.09	38.67	4.58	−1.07 ± 0.11	38.67	5.68	1.60 ± 0.21
43.50	6.70	−0.73 ± 0.09	43.50	5.76	−1.26 ± 0.12	43.50	7.12	1.87 ± 0.26
48.33	8.17	−0.76 ± 0.09	48.33	7.12	−1.47 ± 0.13	48.33	8.72	2.06 ± 0.30
53.17	9.83	−1.29 ± 0.12	53.17	8.66	−1.26 ± 0.12	53.17	10.49	3.38 ± 0.92
58.00	11.70	−1.05 ± 0.12	58.00	10.41	−1.28 ± 0.12			

* Osmotic pressure calculated using equations 2.b.1 and 2.b.2

† ln *K* value determined using the methods described in section 1(b), with errors propagated from equation 2.b.3.

Table S3. Large Osmolyte Effects on ln *K* by Concentration									
PEG 1000			**PEG 1500**				**PEG 2000**		
Wt%	Calc. Π / MPa *	ln *K* †	Wt%	Calc. Π / MPa *	pH 6.5 ln *K* †	pH 7.5 ln *K* †	Wt%	Calc. Π / MPa *	ln *K* †
0.00	0.00	0.47 ± 0.08	0.00	0.00	5.2 ± 3.5	0.54 ± 0.09	0.00	0.00	0.54 ± 0.09
4.83	0.14	0.30 ± 0.08	4.83	0.10	1.73 ± 0.16	0.27 ± 0.08	4.83	0.08	0.11 ± 0.08
9.67	0.35	0.17 ± 0.08	9.67	0.27	0.91 ± 0.10	−0.03 ± 0.10	9.67	0.23	−0.31 ± 0.08
14.50	0.65	−0.11 ± 0.08	14.50	0.53	0.41 ± 0.08	−0.46 ± 0.08	14.50	0.47	−0.30 ± 0.08
19.33	1.05	−0.31 ± 0.08	19.33	0.89	0.36 ± 0.08	−0.49 ± 0.08	19.33	0.81	−0.51 ± 0.09
24.17	1.56	−0.52 ± 0.09	24.17	1.36	0.09 ± 0.08	−0.66 ± 0.08	24.17	1.26	−0.65 ± 0.09
29.00	2.20	−1.31 ± 0.12	29.00	1.96	−0.03 ± 0.08	−1.10 ± 0.08	29.00	1.83	−1.30 ± 0.12
33.83	2.98	−1.62 ± 0.15	33.83	2.69	−0.43 ± 0.08	−1.34 ± 0.08	33.83	2.55	−1.49 ± 0.13
38.67	3.91	−1.77 ± 0.16	38.67	3.58	−0.41 ± 0.08	−1.30 ± 0.08	38.67	3.41	−1.36 ± 0.12
43.50	5.00	−1.67 ± 0.15	43.50	4.63	−0.59 ± 0.09	−1.35 ± 0.09	43.50	4.44	−1.81 ± 0.17
48.33	6.27	−1.60 ± 0.15	48.33	5.85	−0.59 ± 0.10	−1.29 ± 0.10	48.33	5.64	−1.61 ± 0.15
53.17	7.73	−1.70 ± 0.18	53.17	7.26	−0.69 ± 0.13	−1.16 ± 0.13	53.17	7.02	−1.85 ± 0.19
58.00	9.38	−1.63 ± 0.22	58.00	8.87	−0.96 ± 0.19	−1.30 ± 0.19	58.00	8.61	−1.58 ± 0.22

* Osmotic pressure calculated using equations 2.b.1 and 2.b.2

† ln *K* value determined using the methods described in section 1(b), with errors propagated from equation 2.b.3.

Table S4. Additional Large Osmolyte Effects on ln K by Concentration								
PEG 3000			**PEG 4000**			**PEG 6000**		
Wt%	Calc. Π / MPa *	ln K †	Wt%	Calc. Π / MPa *	ln K †	Wt%	Calc. Π / MPa *	ln K †
0.00	0.00	0.53 ± 0.09	0.00	0.00	0.54 ± 0.09	0.00	0.00	0.36 ± 0.08
4.83	0.06	0.27 ± 0.08	4.83	0.05	−0.10 ± 0.08	4.83	0.04	0.27 ± 0.08
9.67	0.19	−0.10 ± 0.08	9.67	0.17	−0.37 ± 0.08	9.67	0.16	−0.10 ± 0.08
14.50	0.41	−0.24 ± 0.08	14.50	0.38	−0.46 ± 0.08	14.50	0.36	−0.24 ± 0.08
19.33	0.73	−0.15 ± 0.08	19.33	0.69	−0.53 ± 0.09	19.33	0.66	−0.15 ± 0.08
24.17	1.16	−0.44 ± 0.08	24.17	1.11	−0.69 ± 0.09	24.17	1.07	−0.44 ± 0.08
29.00	1.71	−0.89 ± 0.10	29.00	1.65	−0.98 ± 0.10	29.00	1.62	−0.89 ± 0.10
33.83	2.40	−0.85 ± 0.10	33.83	2.33	−1.29 ± 0.12	33.83	2.30	−0.85 ± 0.10
38.67	3.25	−1.19 ± 0.12	38.67	3.16	−1.52 ± 0.14	38.67	3.13	−1.02 ± 0.12
43.50	4.25	−1.61 ± 0.14	43.50	4.16	−2.00 ± 0.19	43.50	4.13	−1.38 ± 0.16
48.33	5.43	−1.73 ± 0.16	48.33	5.32	−1.98 ± 0.19	48.33	5.31	−1.72 ± 0.19
53.17	6.79	−1.94 ± 0.20	53.17	6.67	−1.90 ± 0.20			

* Osmotic pressure calculated using equations 2.b.1 and 2.b.2

† ln K value determined using the methods described in section 1(b), with errors propagated from equation 2.b.3.

Table S5. Experimental Rhodopsin Hydration Parameters			
	N_W *	ΔC / MPa^{-2} †	$\Delta\kappa$ / MPa^{-1} †
PEG 200	61 ± 13	0.023 ± 0.009	0.0016 ± 0.0006
PEG 300	70 ± 7	0.045 ± 0.009	0.0031 ± 0.0006
PEG 400	47 ± 8	0.026 ± 0.010	0.0018 ± 0.0007
PEG 600	88 ± 5	0.085 ± 0.007	0.0059 ± 0.0005
PEG 1000	97 ± 10	0.116 ± 0.016	0.0081 ± 0.0011
PEG 1500	78 ± 12	0.10 ± 0.02	0.0072 ± 0.0015
PEG 2000	91 ± 11	0.12 ± 0.02	0.0081 ± 0.0014
PEG 3000	80 ± 11	0.09 ± 0.02	0.006 ± 0.0017
PEG 4000	94 ± 14	0.13 ± 0.03	0.009 ± 0.002
PEG 6000	75 ± 14	0.09 ± 0.03	0.006 ± 0.002

* Numbers of hydrating water molecules for a MI–MII transition under standard conditions. For small osmolytes (i.e., PEG 200 to PEG 600), only the quadratic behavior following the apparent saturation point was utilized in the parameter calculations. Second-degree polynomials were fit in Matlab using a nonlinear least squares regression algorithm, which enabled calculation of both the parameter values (eqs. 2.a.10 and 2.a.17) and their standard errors.

† Change in virial coefficient ΔC or change in compressibility $\Delta\kappa$ for a MI–MII transition under standard conditions, using the same procedure outlined above. See also Figure 1 of the main text.

Table S6. Tabulated pH Titration Data *													
No PEG		PEG 200		PEG 300		PEG 600		PEG 1000		PEG 2000		PEG 4000	
pH	Θ	pH	θ	pH	θ	pH	θ	pH	θ	pH	θ	pH	θ
3.47	0.52	3.27	0.29	3.29	0.47	3.26	0.60	3.29	0.56	3.38	0.56	3.21	0.40
3.89	0.82	3.47	0.36	4.03	0.72	3.69	0.63	3.85	0.61	3.91	0.61	3.62	0.56
4.22	0.94	3.92	0.62	4.50	0.77	3.95	0.66	4.15	0.61	4.32	0.63	4.19	0.58
4.89	1.00	4.43	0.76	4.96	0.79	4.40	0.69	4.69	0.64	4.84	0.61	4.78	0.59
5.34	1.00	4.80	0.83	5.37	0.84	5.05	0.71	5.29	0.62	5.26	0.58	5.10	0.54
5.88	1.00	5.29	0.92	5.72	0.89	5.53	0.65	5.84	0.50	5.55	0.42	5.50	0.49
6.05	1.00	5.71	0.95	5.79	0.88	6.04	0.43	6.08	0.41	5.91	0.40	6.10	0.30
6.58	0.88	6.07	1.00	6.21	0.89	6.59	0.33	6.53	0.26	6.53	0.24	6.70	0.24
7.07	0.75	6.44	1.00	6.62	0.84	7.00	0.29	7.24	0.18	7.14	0.17	7.27	0.15
7.45	0.57	6.87	1.00	7.01	0.83	7.60	0.23	8.36	0.13	7.53	0.14	7.84	0.11
8.04	0.41	7.48	0.95	7.45	0.79	8.11	0.21			7.91	0.14	8.03	0.10
8.46	0.31	7.93	0.87	8.05	0.64	8.51	0.17			8.64	0.10	8.61	0.09
8.95	0.21	8.42	0.76	8.22	0.62	9.01	0.16			9.10	0.09	9.12	0.08
		8.90	0.70	8.79	0.44	9.19	0.15					9.60	0.09

***** MII fractions (θ) are taken from the fitting of basis spectra to the experimental spectra according to the method described in section 1(b). Data are plotted in Figure S6 and main text Figure 4.

Table S7. Rhodopsin pK_A Modulation by Osmolytes *			
	p$K_{A,\,SB}$	p$K_{A,\,Glu}$	θ_{alk}
No PEG	3.3 ± 0.1	7.4 ± 0.2	0.22 ± 0.07
30% (w/w) PEG 200	3.7 ± 0.1	8.2 ± 0.6	0.6 ± 0.2
30% (w/w) PEG 300	3.6 ± 0.3	7.2 ± 0.7	0.5 ± 0.2
50% (w/w) PEG 600	3.4 ± 0.3	5.5 ± 0.3	0.2 ± 0.1
50% (w/w) large PEGs	3.5 ± 0.2	5.2 ± 0.2	0.16 ± 0.05

* Tabulated pK_A values and alkaline endpoints were calculated by fitting eq. 2.e.6 to experimental pH titration data in various osmotic conditions. Also included are the 95% confidence interval errors of each of these parameters as calculated by Matlab R2018a.

4. Supplemental References

1. M. F. Brown, UV-visible and infrared methods for investigating lipid-rhodopsin membrane interactions. *Methods Mol Biol* **914**, 127-153 (2012).
2. R. M. Peitzsch, W. F. Reed, High osmotic stress behavior of hyaluronate and heparin. *Biopolymers* **32**, 219-238 (1992).
3. C. Altenbach, A. K. Kusnetzow, O. P. Ernst, K. P. Hofmann, W. L. Hubbell, High-resolution distance mapping in rhodopsin reveals the pattern of helix movement due to activation. *Proc Natl Acad Sci USA.* **105**, 7439-7444 (2008).
4. J. A. Cohen, R. Podgornik, P. L. Hansen, V. A. Parsegian, A Phenomenological One-Parameter Equation of State for Osmotic Pressures of PEG and Other Neutral Flexible Polymers in Good Solvents. *J Phys Chem B* **113**, 3709-3714 (2009).
5. T. Okada *et al.*, The retinal conformation and its environment in rhodopsin in light of a new 2.2 A crystal structure. *J Mol Biol* **342**, 571-583 (2004).
6. N. R. Voss, M. Gerstein, 3V: Cavity, Channel and Cleft Volume Calculator and Extractor. *Nucleic Acids Res* **38**, W555-W562 (2010).
7. D. C. Mitchell, B. J. Litman, Effect of protein hydration on receptor conformation: decreased levels of bound water promote metarhodopsin II formation. *Biochemistry* **38**, 7617-7623 (1999).
8. D. C. Mitchell, B. J. Litman, Effect of ethanol and osmotic stress on receptor conformation. Reduced water activity amplifies the effect of ethanol on metarhodopsin II formation. *J Biol Chem* **275**, 5355-5360 (2000).
9. N. P. Money, Osmotic Pressure of Aqueous Polyethylene Glycols. *Plant Physiol* **91**, 766-769 (1989).
10. M. Mahalingam, K. Martínez-Mayorga, M. F. Brown, R. Vogel, Two protonation switches control rhodopsin activation in membranes. *Proc Natl Acad Sci USA* **105**, 17795-17800 (2008).